p38 MAPK inhibits autophagy and promotes microglial inflammatory responses by phosphorylating ULK1

Yingli He,[1,2,3]* Hua She,[2,3]* Ting Zhang,[2,3,4] Haidong Xu,[2,3] Lihong Cheng,[3] Manuel Yepes,[3] Yingren Zhao,[1] and Zixu Mao[2,3]

[1]The First Affiliated Hospital of Xi'an Jiaotong University, Xi'an, China
[2]Department of Pharmacology and [3]Department of Neurology, Emory University School of Medicine, Atlanta, GA
[4]Key Laboratory of Environmental Medicine Engineering, School of Public Health, Southeast University, Nanjing, China

Inflammation and autophagy are two critical cellular processes. The relationship between these two processes is complex and includes the suppression of inflammation by autophagy. However, the signaling mechanisms that relieve this autophagy-mediated inhibition of inflammation to permit a beneficial inflammatory response remain unknown. We find that LPS triggers p38α mitogen-activated protein kinase (MAPK)–dependent phosphorylation of ULK1 in microglial cells. This phosphorylation inhibited ULK1 kinase activity, preventing it from binding to the downstream effector ATG13, and reduced autophagy in microglia. Consistently, p38α MAPK activity is required for LPS-induced morphological changes and the production of IL-1β by primary microglia in vitro and in the brain, which correlates with the p38α MAPK-dependent inhibition of autophagy. Furthermore, inhibition of ULK1 alone was sufficient to promote an inflammatory response in the absence of any overt inflammatory stimulation. Thus, our study reveals a molecular mechanism that enables the initial TLR4-triggered signaling pathway to inhibit autophagy and optimize inflammatory responses, providing new understanding into the mechanistic basis of the neuroinflammatory process.

Introduction

Dysfunction of autophagy and inflammation has been implicated in the pathogenic process of a growing list of neurodegenerative diseases (Netea-Maier et al., 2016). Autophagy and inflammation are highly intertwined cellular processes (Levine et al., 2011). Autophagy plays an antiinflammatory role and suppresses proinflammatory process through regulating innate immune signaling pathways and inflammasome activity (Deretic et al., 2013). Inflammatory signals also function to reciprocally control autophagy (Shi et al., 2012). However, the mechanisms by which inflammatory signals specifically relieve the negative suppression by autophagy on inflammation remain unknown. In this study, we show that p38α MAPK plays a direct and essential role in relieving autophagic control in response to inflammatory signal. We found that upon lipopolysaccharide (LPS) stimulation, p38α MAPK directly phosphorylates UNC51-like kinase-1 (ULK1), the serine/threonine kinase in the initiation complex of the autophagic cascade, in microglia. Phosphorylation by p38α MAPK inhibited ULK1 activity and disrupted its interaction with autophagy-related protein 13 (ATG13) in the autophagy initiation complex and reduced the flux and level of autophagy. This inhibition is necessary for LPS-induced inflammasome activity, interleukin-1β (IL-1β) production, and microglial activation in culture and in the mouse brain. Thus, our findings establish a mechanism that functions to relieve the immune-suppressive activity of autophagy upon stimulation and allows the full induction of inflammatory process during microglial activation. This mechanism may play an important role in regulating innate immune response in the nervous system.

Results

LPS inhibits autophagy in microglia

To understand the mechanism of how signals control and release autophagic suppression of inflammation, we first tested whether LPS modulates autophagy in microglia. We treated the murine microglial cell BV2, a model cell widely used in neuroinflammation research (Blasi et al., 1990), with LPS and found that this caused a dose-dependent decrease in the level of autophagy marker LC3-II, the lipidated form of the microtubule-associated proteins 1A/1B-light chain 3 (LC3), as well as an increase in the level of autophagy adapter protein p62 but not its mRNA (Figs. 1 A and S1 A; Jain et al., 2010; Fujita et al., 2011; Klionsky et

*Y. He and H. She contributed equally to this paper.

Correspondence to Zixu Mao: zmao@emory.edu; Yingren Zhao: zhaoyingren@mail.xjtu.edu.cn

The Rockefeller University Press
J. Cell Biol. Vol. 217 No. 1 315–328
https://doi.org/10.1083/jcb.201701049

al., 2012). The change in LC3-II correlated closely with a steady increase in the levels of activated caspase-1 and mature IL-1β in cell lysates and in culture media (Figs. 1 A and S1 A), indicating inflammatory activation of BV2. To confirm the effect of LPS on LC3-II, we overexpressed GFP-LC3 in BV2 cells and showed that LPS inhibited the conversion of GFP–LC3-I to GFP–LC3-II in a time-dependent manner (Fig. 1 B). Exposure to bafilomycin A1 (BA), which blocks the fusion of autophagosomes with lysosomes (Yamamoto et al., 1998), caused a significant accumulation of LC3-II in BV2 cells. Cotreatment of the cells with LPS greatly reduced BA-induced LC3-II accumulation (Fig. 1 C). In addition, LPS also attenuated a rapamycin-induced increase in LC3-II as well as a decrease in p62 protein but not its mRNA in both BV2 cells and primary microglia (Fig. 1, D and E; and Fig. S1 B). Furthermore, LPS reduced the number of autophagosomes in BV2 cells (Fig. S1 C). Collectively, these findings suggest that LPS reduces the autophagic flux in microglial cells. Interestingly, LPS did not significantly alter LC3-II level with or without BA in either primary cortical neurons or astrocytes (Fig. 1 F). In addition, when applied to RAW264.7 cells, a widely used macrophage cell model, instead of decreasing LC3-II, LPS enhanced LC3-II (Fig. S1 D), a finding consistent with previous studies (Xu et al., 2007; Delgado et al., 2008). Thus, the inhibitory effect of LPS on autophagy appears to be specific for microglia. Based on these findings, we used BV2 as our primary model to further explore the mechanism underlying LPS-induced inhibition of autophagy as well as its role in microglial inflammatory response.

LPS inhibits autophagy through p38α MAPK

LPS is known to engage toll-like receptor 4 (TLR4) and p38 MAPK in inducing inflammatory response (Bachstetter and Van Eldik, 2010; Bachstetter et al., 2011). We showed that interfering TLR4 activity with either the viral inhibitory peptide VIP ER or the antibiotic polymyxin B, both of which block TLR4-LPS signaling, completely abrogated the inhibitory effect of LPS on autophagy (Fig. S1, E and F). In contrast, peptidoglycan, a TLR2 agonist, weakly activated p38α and had little effect on autophagy in BV2 cells (Fig. S1 G). To test the role of p38 MAPK in LPS-induced inhibition of autophagy, we cotreated BV2 cells with LPS and SB203580, a chemical inhibitor of p38 MAPK. This analysis showed that, correlated with its effects on LC3-II and p62, LPS induced a robust activation of p38α MAPK, indicated by its increased phosphorylation (Figs. 2 A and S2 A). These LPS-induced changes were clearly attenuated by SB203580. Similarly, specific knockdown p38α MAPK by siRNA also prevented LPS-induced changes in the levels of LC3-II and p62 protein but not p62 mRNA (Figs. 2 B and S2 B). However, increasing p38 MAPK activity by its small molecule activator anisomycin (AN; Zhu et al., 2005) was sufficient to significantly reduce the level of endogenous LC3-II, which was blocked by SB203580 (Fig. 2 C, top). In addition, AN also greatly attenuated BA-induced accumulation of LC3-II (Fig. 2 C, bottom). To corroborate with these findings, we tested the effect of expressing p38α MAPK on LC3 lipidation. For this study, we expressed GFP-LC3 and determined the generation of free GFP after the lysosomal-dependent turnover of GFP-LC3 (Rubinsztein et al., 2009; Mizushima et al., 2010). This study revealed that the level of free GFP, which correlates positively with autophagy activity, was reduced by coexpression of p38α MAPK (Fig. 2 D). To strengthen these findings, we used an autophagy sensor, tandem-fluorescently tagged LC3 (mTagRFP-mWasabi-LC3; Kimura et al., 2007; Zhou et al., 2012), to monitor autophagic flux under our experimental condition. We expressed mTagRFP-mWasabi-LC3 in BV2 cells, treated the cells with SB203580 or p38α MAPK knockdown, and scored the green and red puncta. This analysis showed that inhibition of p38 MAPK by SB203580 or knockdown of p38α MAPK led to a significant increase in the number of red puncta (Figs. 2 E and S2 C), consistent with an increase in autophagic flux. Collectively, these findings indicate that p38α MAPK reduces autophagic flux under basal condition and is required for mediating LPS-induced inhibition of autophagy.

p38α MAPK interacts directly with ULK1

Inflammatory signal activates p38 MAPK, but its role has not been fully defined (Doyle et al., 2011; Matsuzawa et al., 2012). Because ULK1 is a key regulator that functions upstream in the autophagic cascade and is regulated via phosphorylation by several kinases in response to nutrient signals (Kim et al., 2011), we tested the possibility that p38α MAPK may regulate autophagy process by directly targeting ULK1. First, we examined whether p38 MAPK may directly interact with ULK1 by an in vitro binding assay. We coincubated purified ULK1 with purified p38α MAPK, immunoprecipitated this with an anti-p38α MAPK antibody, and analyzed the precipitate by anti-ULK1 immunoblotting or performed the coimmunoprecipitation (co-IP) in reverse. This analysis showed that ULK1 and p38α MAPK directly associated with each other (Fig. 3 A). We then expressed MYC-ULK1 and FLAG-p38α MAPK in HEK293 cells, immunoprecipitated them with an anti-MYC antibody, and blotted the precipitate with an anti-FLAG antibody or performed the co-IP in reverse. Data from this analysis indicated that ULK1 and p38α MAPK interacted with each other in cellular lysates (Fig. 3 B). Analysis of ULK1 deletion mutants by co-IP showed that this interaction requires the C terminus of ULK1 (Figs. 3 C and S2 D). Next, we demonstrated by co-IP assay that endogenous ULK1 and p38α MAPK formed a complex in HEK293 and BV2 cells (Fig. 3, D and E) and that LPS treatment did not significantly affect their interaction (Fig. S2 E).

p38α MAPK phosphorylates ULK1

Consistent with the possibility that p38α MAPK may regulate ULK1 activity, we found that coexpression with p38α MAPK caused ULK1 to migrate at a higher-molecular-weight position (Fig. 4 A). This change in ULK1 migration could be reversed by pretreatment of the lysates with the λ phosphatase (λPPase) or treating the cells with SB203580 (Fig. 4, A and B), supporting the possibility that a high level of p38α MAPK activity may result in ULK1 phosphorylation. In support of this, blotting the ULK1 precipitates with an antiphosphoserine antibody revealed an increase in the phosphoserine signal in ULK1 after p38α MAPK expression (Fig. 4 C). Sequence analysis of ULK1 uncovered the presence of several putative p38 MAPK phosphorylation sites conserved among several species (Fig. S3 A). In vitro kinase assay demonstrated that purified p38α MAPK directly phosphorylated the C-terminal portion of ULK1 immunoisolated from cellular lysates (Figs. 4 D and S3 B). Mutation analysis identified serine residues at 504 and 757 as the sites required for p38α MAPK–mediated ULK1 phosphorylation and a shift in migration (Fig. 4, E and F). Analysis of the cellular lysates with a phospho-S757–specific antibody showed that expression of p38α MAPK correlated with increased phosphorylation of ULK1 at S757 (Fig. S3 C). Because mTOR has been

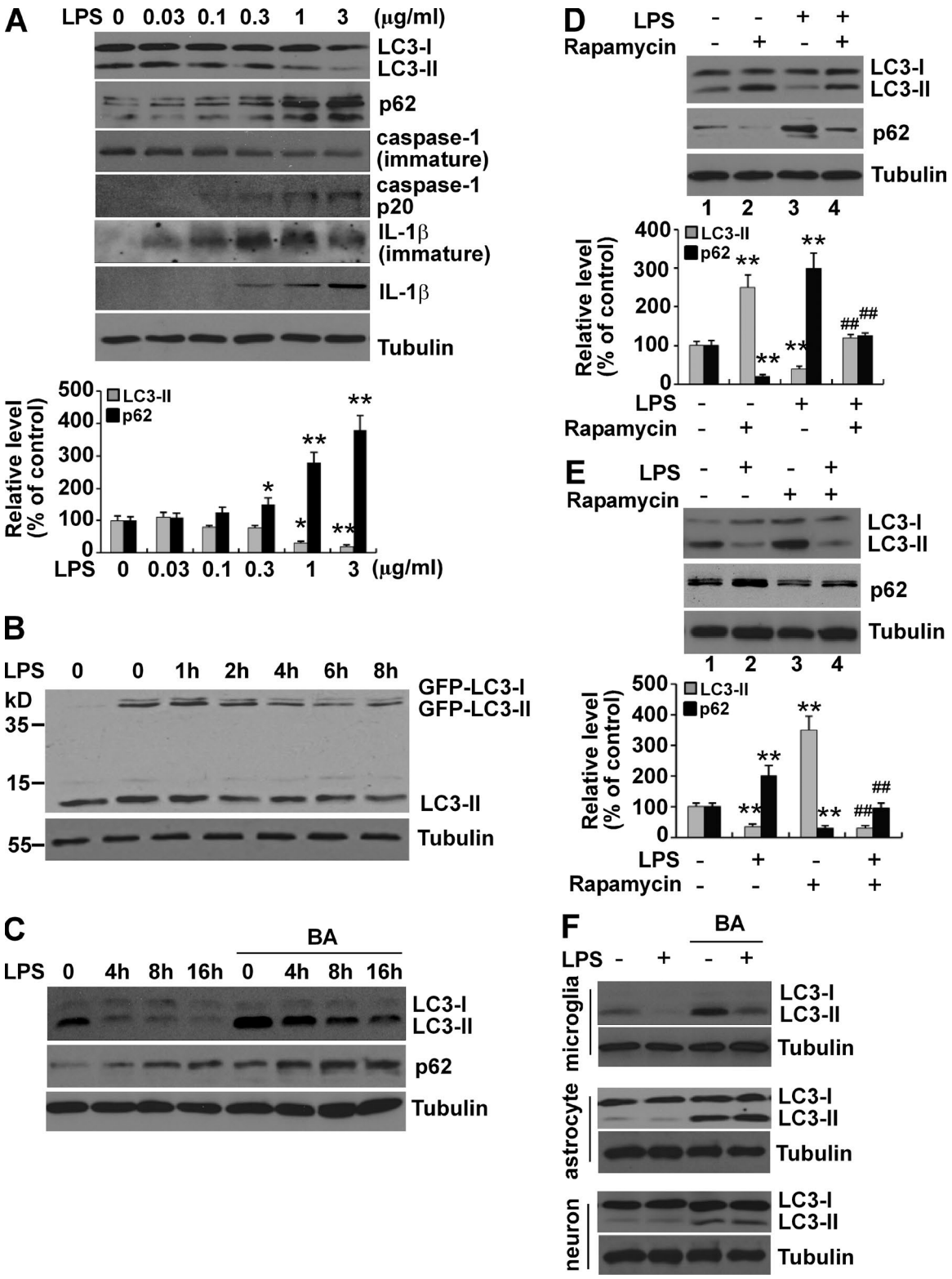

Figure 1. **LPS inhibits autophagy in microglia. (A)** LPS inhibits autophagy in microglial cell line BV2 and activates BV2 cells. BV2 cells were treated with different concentrations of LPS for 8 h. The levels of LC3, p62, caspase-1, and IL-1β were assessed by Western blotting. The bottom graph shows the relative changes of LC3-II and p62 over control. **(B)** LPS inhibits the lipidation of GFP-LC3. BV2 cells transfected with GFP-LC3 were treated with LPS (1 μg/ml) for 0–8 h and blotted with an anti-LC3 antibody. **(C)** LPS inhibits autophagic flux in BV2 cells. BV2 cells were incubated with LPS (1 μg/ml) for 0–16 h and treated with or without BA (100 nM) for the last 4 h. **(D)** LPS inhibits rapamycin-induced autophagy in BV2 cells. BV2 cells were treated with LPS (1 μg/ml), rapamycin (50 nM), or both for 8 h. The bottom graph shows relative changes of LC3-II and p62. **(E)** LPS inhibits rapamycin-induced autophagy in primary microglial cells. Primary microglia were treated as described in D. **(F)** LPS inhibits autophagy specifically in microglial cells. Primary microglia, primary astrocytes, and primary cortical neurons isolated from rat brains were treated with LPS (1 μg/ml) for 8 h with or without BA (100 nM) for the last 4 h. *, $P < 0.05$; **, $P < 0.01$ versus control; ##, $P < 0.01$ versus rapamycin. $n = 4$. Error bars show SD.

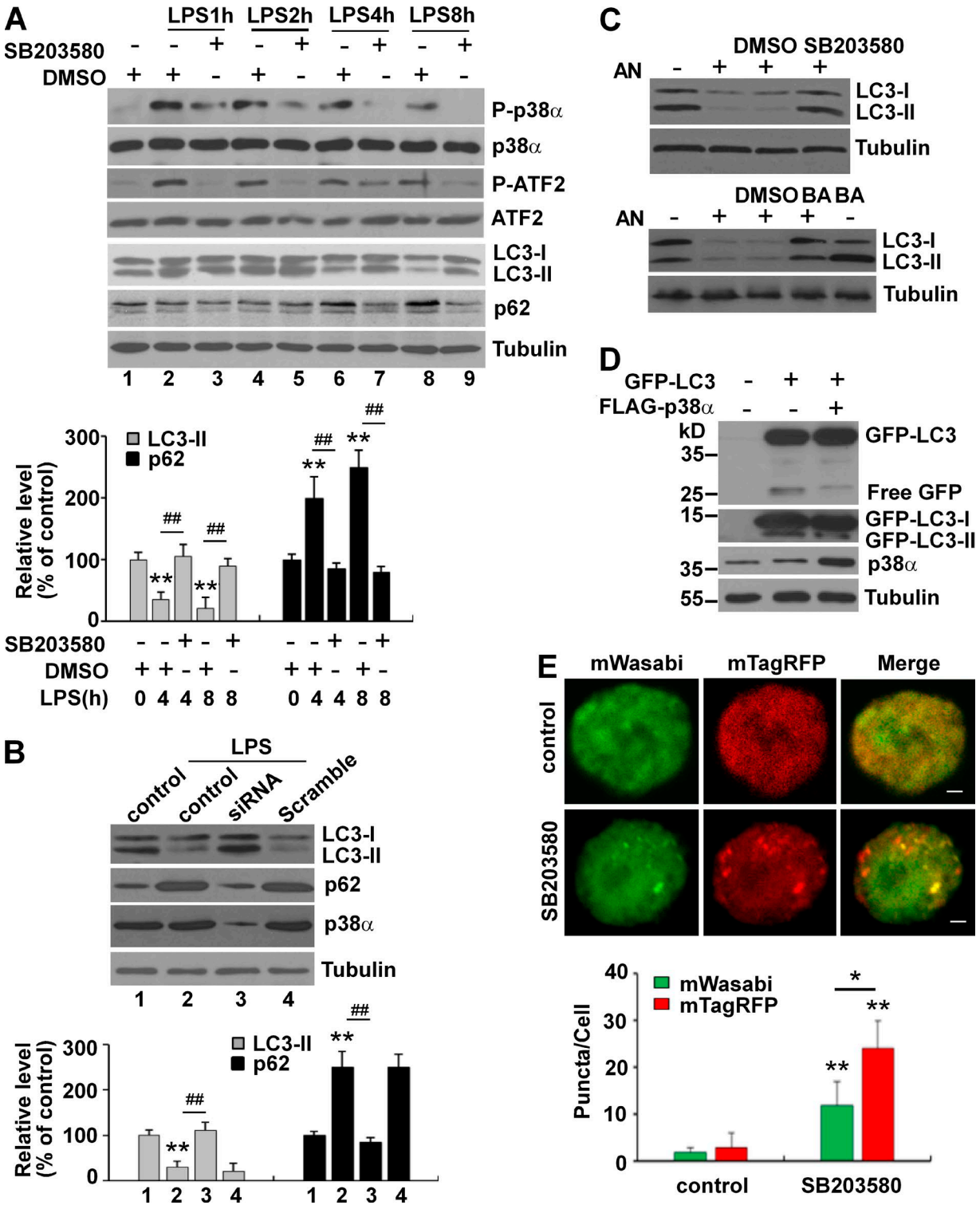

Figure 2. **LPS inhibits autophagy in BV2 cells through p38α MAPK. (A)** p38 MAPK inhibitor SB203580 blocks LPS-induced inhibition of autophagy in BV2 cells. BV2 cells were treated with LPS (1 µg/ml) with or without SB203580 (10 µM) as indicated. The graph below shows relative changes of LC3-II and p62. **(B)** Knockdown of p38α MAPK blocks LPS-induced inhibition of autophagy in BV2 cells. BV2 cells were transfected with scramble or p38 MAPK–specific siRNA for 48 h and then treated with LPS (1 µg/ml) for 8 h. Whole-cell lysates were analyzed by immunoblotting. The graph below shows relative changes of LC3-II and p62. **(C)** The p38 MAPK activator AN inhibits autophagy in BV2 cells. BV2 cells were treated with AN (10 µM) with or without SB203580 (10 µM; top) for 8 h or were treated first with AN for 4 h and then with or without BA (100 nM; bottom) for another 4 h. **(D)** Expression of p38α MAPK reduces the conversion of GFP-LC3. HEK293 cells were transfected with GFP-LC3 or in combination with p38α MAPK for 24 h. Whole-cell lysates were analyzed by immunoblotting. **(E)** SB203580 enhances autophagy in BV2 cells under basal conditions. BV2 cells were transfected with tandem-fluorescently tagged LC3 (mTagRFP-mWasabi-LC3) for 24 h. Cells were treated with or without SB203580 (10 µM) for 8 h. *, $P < 0.05$; **, $P < 0.01$ versus control; ##, $P < 0.01$ versus LPS alone. Bars, 10 µm. $n = 100$. Experiments were repeated three times. Error bars show SD.

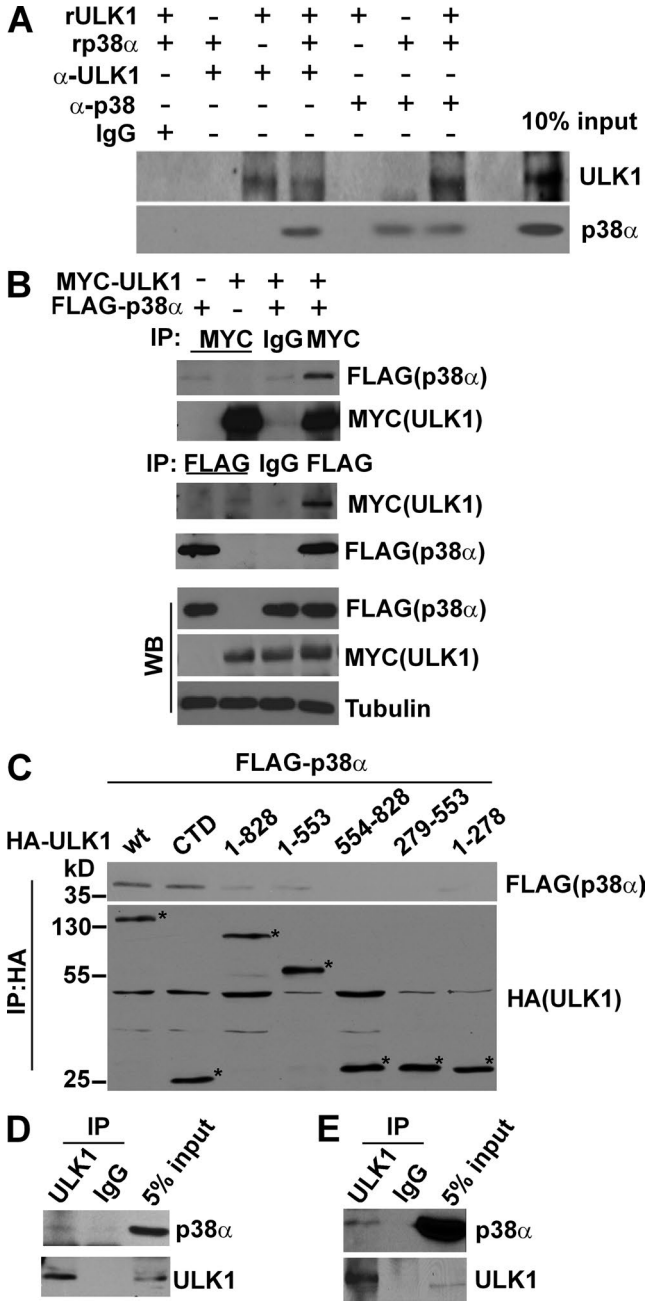

Figure 3. **p38α MAPK interacts with ULK1. (A)** Recombinant p38α MAPK and ULK1 interact with each other in vitro. Recombinant p38α MAPK (50 ng) was incubated with recombinant ULK1 (50 ng) in IP buffer at 4°C for 2 h. Pulldown assays were performed by using an anti–p38α MAPK antibody and blotted with an anti-ULK1 antibody. **(B)** Expressed p38α MAPK and ULK1 interact with each other. FLAG-p38α MAPK and/or MYC-ULK1 were overexpressed in HEK293 cells (bottom). Co-IP was performed by incubating whole-cell lysates (200 µg) with either an anti-MYC or an anti-FLAG antibody (top and middle). WB, Western blot. **(C)** p38α MAPK interacts with the ULK1 C terminus. HA-tagged WT ULK1 or ULK1 fragments were coexpressed with FLAG–p38α MAPK in HEK293 cells. The level of FLAG–p38α MAPK coimmunoprecipitated with HA-ULK1 from 200 µg cell lysates was analyzed with an anti-FLAG antibody. CTD, C-terminal domain. Asterisks denote HA-ULK1 fragments. **(D and E)** Endogenous p38α MAPK and ULK1 interact with each other in HEK293 (D) and BV2 cells (E). Co-IP was performed by incubating whole-cell lysates (400 µg) with anti-ULK1 antibody, and the precipitates were blotted with anti-p38 antibody.

reported to phosphorylate ULK1 at serine 757 after nutrient signaling (Kim et al., 2011), we tested whether mTOR may be involved in phosphorylating ULK1 in response to LPS. Detailed time course analysis of p38α MAPK and mTOR showed that LPS increased the activity of both p38α MAPK and mTOR kinase, with the peak activation of p38α MAPK clearly preceding the phosphorylation of ULK1 (Fig. S3 D). Furthermore, SB203580 attenuated LPS-induced phosphorylation of ULK1 at S757 without significantly affecting the activity of mTOR (Figs. 4 G and S3, E and F). In contrast, the mTOR inhibitor rapamycin did not alter S757 phosphorylation induced by either LPS treatment or expression of p38 MAPK (Fig. S3, E and F). Collectively, these data demonstrate that LPS induces a p38α MAPK– but not mTOR-dependent phosphorylation of ULK1.

Phosphorylation by p38α MAPK reduces ULK1 kinase activity and disrupts the ULK1–ATG13 complex

To assess the effect of phosphorylation by p38α MAPK on ULK1, we expressed p38α MAPK and ULK1, immunoprecipitated ULK1, and measured ULK1 activity by in vitro kinase assay using myelin basic protein (MBP) as a substrate. This study showed that p38α MAPK caused a dose-dependent inhibition of ULK1 kinase activity (Fig. 5 A). Similarly, we treated BV2 cells with LPS, immunoprecipitated endogenous ULK1, and showed by in vitro kinase assay that LPS treatment resulted in a time-dependent decrease in ULK1 kinase activity (Fig. 5 B). SB203580 blocked the inhibitory effect of LPS on ULK1 kinase (Fig. S4 A). ULK1 is known to function in a complex with and phosphorylate ATG13 at S318 (Chan et al., 2009; Hosokawa et al., 2009). We expressed ATG13, ULK1, and p38α MAPK and measured ATG13 and ULK1 binding by co-IP and ATG13 phosphorylation using a phospho-S318–specific antibody. This study showed that p38α MAPK led to a dose-dependent disruption of ATG13–ULK1 interaction and reduced phosphorylation of ATG13 at S318 (Figs. 5 C and S4 B). Either SB203580 or coexpression of a dominant-negative p38α MAPK (p38αDN) reversed the effect of p38α MAPK on ATG13 (Figs. 5 D and S4 C). In contrast to WT ULK1, the binding to ATG13 by ULK1 mutants, which were resistant to p38α MAPK phosphorylation, was far less sensitive to p38α MAPK–induced disruption (Fig. S4 D). Moreover, LPS treatment reduced the interaction of endogenous ULK1 and ATG13 and inhibition of p38 MAPK by SB203580, or knockdown of p38α MAPK abolished the effects of LPS on ATG13 (Fig. 5, E and F). Thus, LPS-induced phosphorylation of ULK1 by p38α MAPK inhibits its kinase activity and disrupts its interaction with and phosphorylation of ATG13.

LPS activates microglia through p38α-mediated inhibition of autophagy

We next studied the role of p38α MAPK-mediated phosphorylation of ULK1 in the LPS-induced microglial inflammatory response. First, we found that LPS-induced inhibition of autophagy correlated closely with a dose- and time-dependent increase of inflammatory response in primary microglia (Figs. 6 A and S5, A and B) and BV2 cells (Fig. S5, C and D). Microglial activation after TLR4 engagement by various pathological stimuli is typified by changes in microglial morphology such as process retraction and cell body enlargement in addition to biochemical changes such as caspase-1 activation (Kettenmann et al., 2011). Next, we recapitulated the finding that LPS-induced the cell

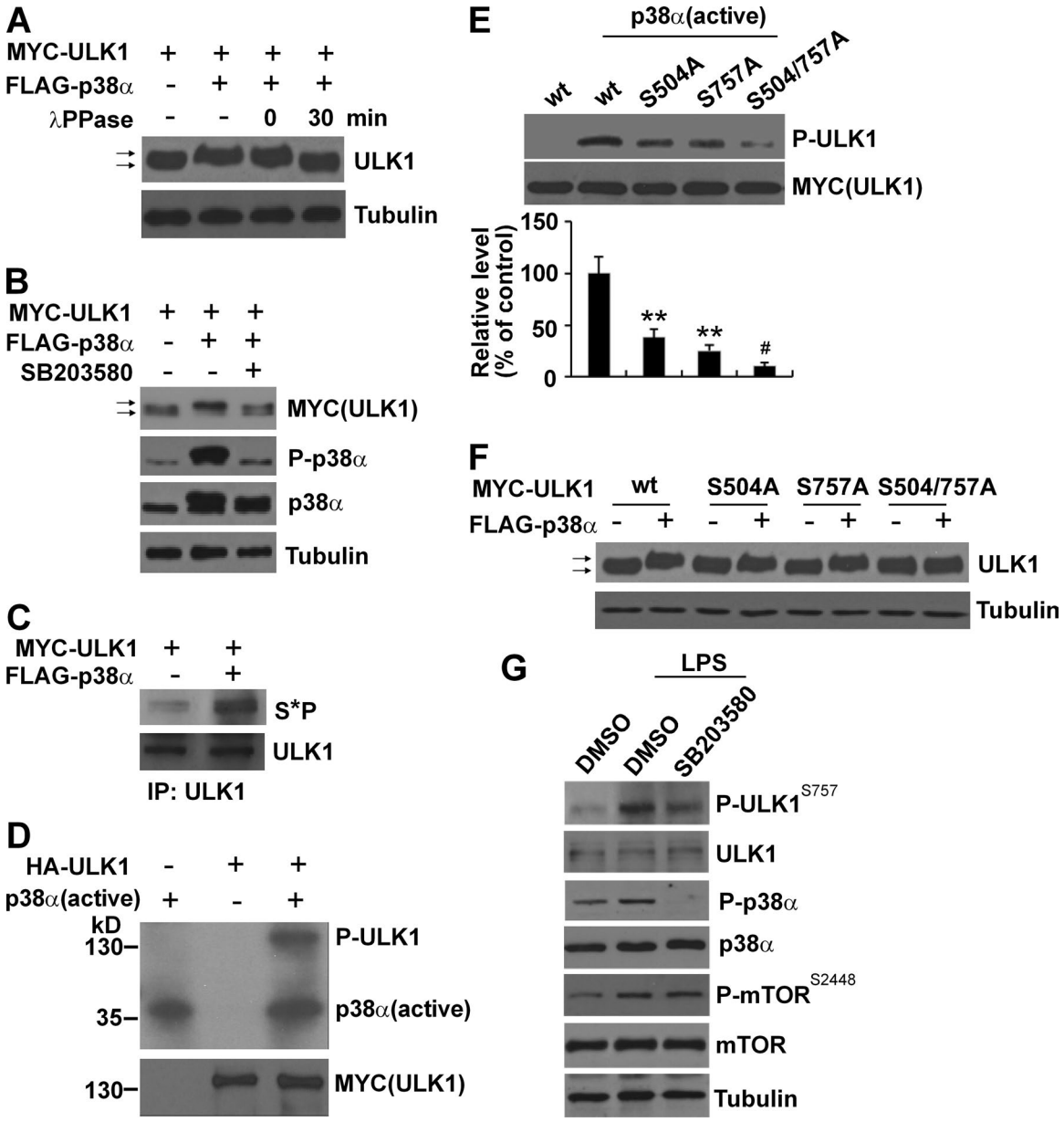

Figure 4. **p38α MAPK phosphorylates ULK1. (A)** p38α MAPK induces a shift in ULK1 migration. Coexpression of ULK1 and p38α MAPK in BV2 resulted in an upshift of ULK1 migration. Pretreatment of the lysates with λPPase for 30 min reversed this effect. **(B)** Coexpression of p38α MAPK and ULK1 in HEK293 cells leads to a shift in ULK1 migration, and SB203580 (10 µM) reverses this effect. **(C)** Coexpression of p38α MAPK leads to ULK1 phosphorylation at serine residues. HEK293 cells were transfected with ULK1 with or without p38α MAPK. The lysates were precipitated with an anti-ULK1 antibody and analyzed with an antibody that specifically recognizes the phosphorylated serine residues followed by a proline (S*P). **(D)** p38α MAPK directly phosphorylates ULK1. ULK1 was expressed in HEK293 cells and immunoprecipitated. The precipitates were incubated with or without a purified active p38α MAPK in in vitro kinase assay. **(E)** p38α MAPK phosphorylates ULK1 at S504 and S757. ULK1 WT and various mutants were expressed and immunoprecipitated. The precipitates were incubated with a purified active p38α MAPK in in vitro kinase assay. Mutation of both serines 504 and 757 to alanine (S504/S757A) reduced the p38α MAPK–induced ULK1 phosphorylation. **(F)** Mutation of ULK1 at S504/S757 blocks the p38α MAPK–induced shift in ULK1 migration. **(G)** p38α MAPK is required for mediating LPS-induced phosphorylation of ULK1. BV2 cells were treated with LPS (1 µg/ml) with or without SB203580 (10 µM) for 2 h. Lysates were blotted as shown. Arrows indicate band shifts. **, $P < 0.01$ versus control; #, $P < 0.05$ versus S504A or S757A. $n = 3$. Error bars show SD.

body roundness and enlargement in cultured primary microglia and showed that SB203580 significantly attenuated the effects of LPS on the microglial morphology (Fig. 6 B). Inflammasome is known to control caspase-1 activation and IL-1β production. Because the core inflammasome components NLRP3 and ASC were detectable in our model (Fig. S5 E), we tested the effect of the NLRP3 inflammasome inhibitor glyburide (Lamkanfi et al., 2009) and found that it significantly attenuated LPS-induced caspase-1 activation and IL-1β production but had no effect on LPS-induced decrease of LC3-II (Figs. 6 C and S5 F). In contrast to glyburide, SB203580 or knockdown of p38α MAPK significantly attenuated LPS-induced decrease in LC3-II while reducing LPS-induced activation of caspase-1 and increase of IL-1β and IL-18 (Figs. 6 C and S5, F and G). To establish the role of inhibition of ULK1 in the inflammatory response, we treated primary microglia with the ULK1 inhibitor MRT67307 (Petherick

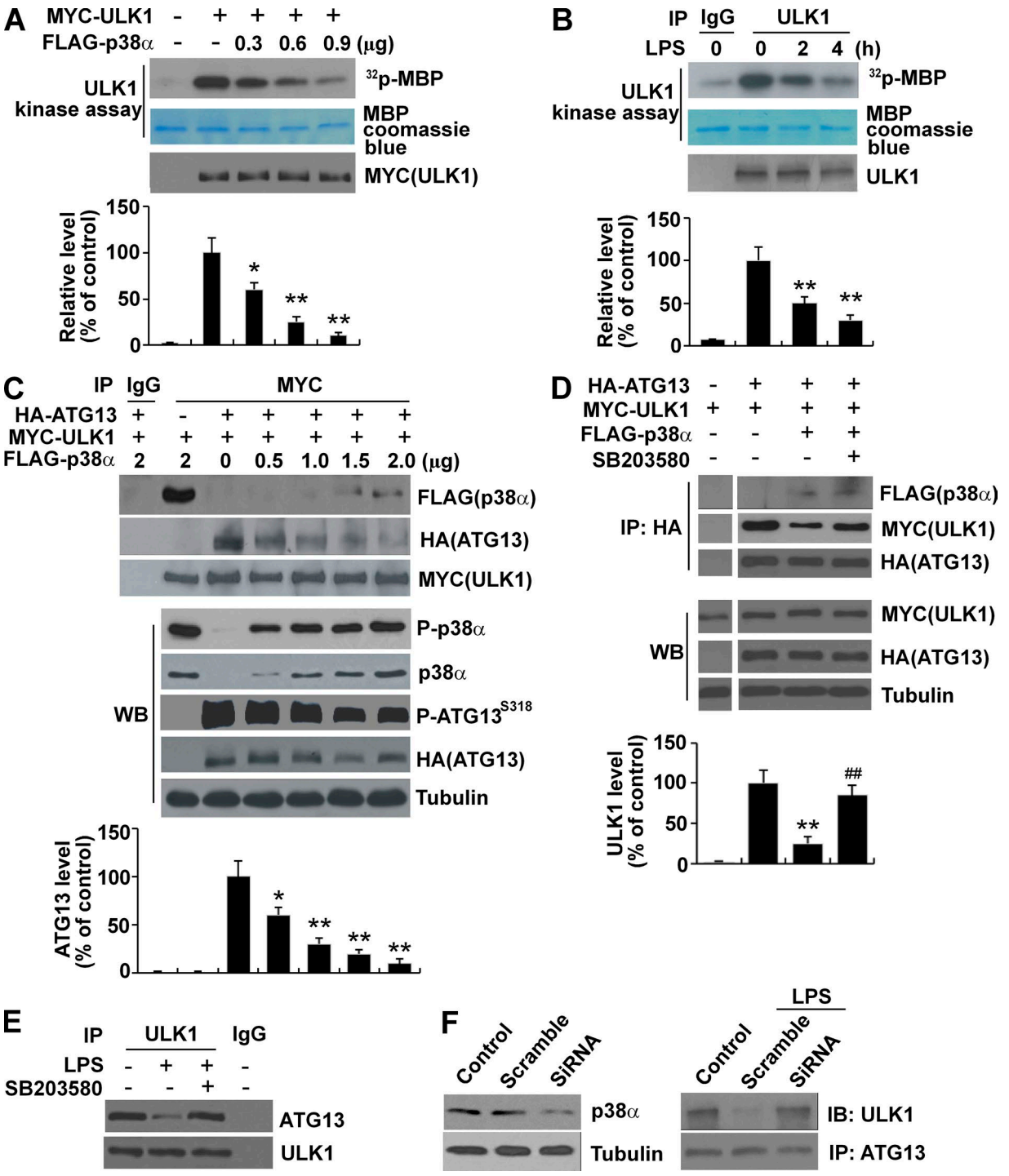

Figure 5. **Phosphorylation by p38α MAPK reduces ULK1 kinase activity and disrupts the ULK1–ATG13 complex. (A)** Expression of p38α MAPK reduces ULK1 kinase activity. MYC-ULK1 with different amounts of FLAG–p38α MAPK was cotransfected into HEK293 cells for 24 h. The activity of immunoprecipitated MYC-ULK1 was measured by in vitro kinase assay using MBP as the substrate. The bottom graph shows relative change of [^{32}P]-MBP signal. **(B)** LPS treatment reduces ULK1 kinase activity. BV2 cells were treated with LPS (1 μg/ml) for the indicated time. Endogenous ULK1 was immunoprecipitated and analyzed by in vitro kinase assay. **(C)** p38α MAPK disrupts the ULK1–ATG13 complex and reduces ATG13 phosphorylation. ATG13 and ULK1 were coexpressed with or without coexpression of p38α MAPK in HEK293 for 24 h. The whole-cellular lysates (200 μg) were immunoprecipitated with an anti-MYC antibody, and the precipitates were blotted with an anti-HA or anti-FLAG antibody (top). The levels of phosphorylated ATG13 (S318) were determined using a phospho-S318–specific antibody (bottom). **(D)** SB203580 blocks p38α MAPK–induced ULK1–ATG13 complex disruption. BV2 cells were treated as described in C with the presence of SB203580 (10 μM). Co-IP was performed by incubating whole-cell lysates (200 μg) with an anti-HA antibody. WB, Western blot. **(E)** SB203580 blocks LPS (1 μg/ml)-induced disruption of the endogenous ULK1–ATG13 complex. BV2 cells were treated with LPS (1 μg/ml) with or without SB203580 (10 μM) for 2 h. Co-IP was performed by incubating whole-cell lysates (400 μg) with an anti-ULK1 antibody. **(F)** Knockdown of p38α MAPK blocks LPS (1 μg/ml)-induced disruption of the endogenous ULK1–ATG13 complex. BV2 cells were transfected with scramble or p38α MAPK–specific siRNA for 48 h and treated with LPS (1 μg/ml) for 2 h. Co-IP was performed by incubating whole-cell lysates (400 μg) with an anti-ATG13 antibody. The left panel shows the effect of knockdown. IB, immunoblot. *, $P < 0.05$; **, $P < 0.01$ versus control; ##, $P < 0.01$ versus p38α. $n = 3$. Error bars show SD.

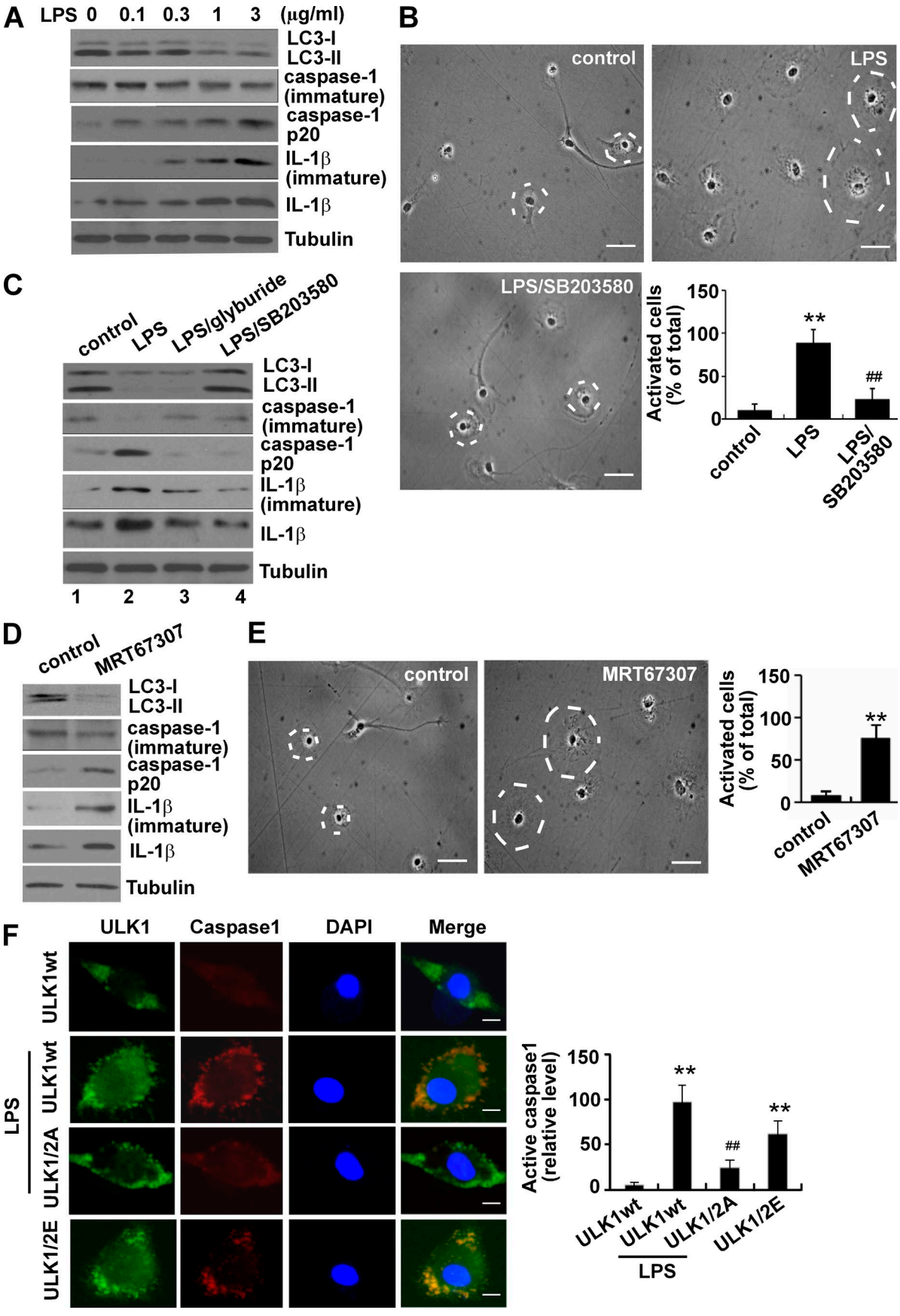

et al., 2015) and measured its effects. This analysis showed that inhibition of ULK1 under basal conditions caused enlargement of the microglial cell body, reduced the level of LC3-II, activated caspase-1, and increased the level of IL-1β (Fig. 6, D and E; and Fig. S5 H). To further confirm the role of ULK1 in LPS-induced microglia activation, we transfected primary microglia with WT ULK1 or the p38α phosphorylation site mutant ULK1 (ULK1/wt, ULK1/2A, and ULK1/2E, respectively), treated cells with LPS, and analyzed caspase-1 activation in situ by immunocytochemistry. The results showed that LPS-induced caspase-1 activation was much lower in cells expressing ULK1/2A than ULK1-WT, and expression of phosphorylation mimicking ULK1 (ULK1/2E) alone could induce caspase-1 activation (Fig. 6 F). Expression of ULK1 mutants by lentivirus in primary microglial cells revealed that compared with WT, ULK1/2A was more effective in attenuating LPS-induced LC3-II decrease and production of IL-1β, whereas ULK1/2E exacerbated the effects of LPS on LC3-II and IL-1β (Fig. S5 I).

To further evaluate the role of autophagy inhibition in LPS-induced microglia activation, we blocked autophagy in cultured primary microglia by knockdown of the essential autophagy gene *ATG5* or with the autophagy inhibitor 3-methyladenine (3-MA). The results showed that knockdown of *ATG5* or treatment with 3-MA under basal conditions induced microglial activation (Fig. 7, A and B; and Fig. S6, A–C). To confirm these findings in vivo, we injected mice with 3-MA by i.p. Analysis of mouse cortical brain tissues showed that under basal conditions, 3-MA reduced the level of LC3-II and increased the levels of p62, caspase-1, IL-1β, and Iba1, a marker for activated microglia (Fig. 7, C and D). We then injected LPS directly into mouse brain by intracerebroventricular injection (I.C.V.) with or without prior injection of SB203580 (i.p.). Analysis of the cortical brain tissues revealed that LPS activated p38α MAPK, led to ULK1 phosphorylation at S757, reduced the level of LC3-II, and increased the levels of caspase-1, IL-1β, and Iba1 (Fig. 7, E and F). Administration of SB203580 clearly attenuated the LPS-induced effects on ULK1, LC3-II, caspase-1, IL-1β, and Iba1. In addition, analysis of autophagosomes with monodansylcadaverine (MDC; Iwai-Kanai et al., 2008) showed that SB203580 reversed LPS-induced reduction of autophagosomes in the mouse brain (Fig. S6 D). Thus, p38α MAPK–dependent phosphorylation and inhibition of ULK1 and autophagy play a critical role in mediating LPS-induced microglial activation and production of inflammatory cytokine in vivo.

Discussion

Autophagy is known to negatively control inflammasome activity in innate immune cells under basal conditions (Harris et al., 2011; Deretic et al., 2013). A decrease in autophagic activity in these cells correlates positively with the inflammatory response (Zhou et al., 2011; Lapaquette et al., 2012; Ravindran et al., 2016). But the mechanisms through which proinflammatory signals regulate autophagy in innate immune cells including microglia remain elusive. Nor is it clear whether such a regulation is required for inflammatory reaction in these cells. Using microglial inflammatory response as a model, we have revealed in this study a central mechanism by which proinflammatory signals exemplified by LPS relieves the tight inhibitory control exerted by autophagy on the inflammatory process. Our findings show that in response to proinflammatory signal, p38α MAPK directly phosphorylates ULK1, inhibits its kinase activity, disrupts its functional complex with ATG13, and reduces autophagy. Because ULK1 is the key upstream regulator of the autophagy pathway, our model suggests that proinflammatory signal engages autophagy at one of the earliest steps of the entire process to allow more efficient removal of the inhibition during microglial activation.

Furthermore, our data suggest that under basal condition, autophagy appears to exert a constant and powerful repression on the microglial inflammatory machinery. In the absence of overt proinflammatory signals such as LPS stimulation, either increasing p38 MAPK activity or reducing ULK1 and autophagy activity alone is sufficient to trigger microglial activation including cellular morphological and biochemical changes in culture and in the brain. Thus, modulating the activity of p38α MAPK–ULK1 axis appears to be sufficient to alter inflammatory status of microglial cells. This would be consistent with the idea that the default mode of inflammatory machinery in microglia is already set at a stage allowing it to function once the inhibitory control is disengaged. In support of this, our data show that there is a detectable level of NLRP3 and ASC interaction in BV2 cells under basal condition. It is certainly possible that there are additional mechanisms that either in parallel or in sequence to the p38 MAPK–ULK1 pathway negatively control the inflammatory machinery. Our finding that engaging ULK1 by p38 MAPK is obligatory and sufficient to modulate microglial inflammatory response indicates that p38 MAPK–mediated regulation of ULK1 should represent a major upstream mechanism central in the inflammatory process.

One of the surprising and intriguing findings from our study is the differential LC3 response to LPS between microglial BV2 cells and macrophage RAW264.7 cells. Several studies have reported that activation of TLR4 or 7 activates autophagy in primary macrophages and the macrophage cell line (Xu et al., 2007; Delgado et al., 2008). Consistent with these, we also found that unlike in BV2 cells, LPS increased the level of LC3-II in RAW264.7. Although the precise reason for the different findings between these studies and ours is not clear, part

Figure 6. **LPS activates microglia through the p38α MAPK–ULK1 pathway. (A)** LPS reduces LC3-II level in primary microglia and induces the microglial inflammatory response. Primary microglia were treated with different concentrations of LPS for 8 h. The levels of LC3, caspase-1, and IL-1β were assessed by Western blotting. **(B)** SB203580 blocks LPS-induced morphological change in cultured primary microglia. Primary microglia were treated with LPS (1 µg/ml) with or without SB203580 (10 µM) for 12 h and scored for process retraction and cell body enlargement. **(C)** Glyburide or SB203580 blocks LPS-induced caspase-1 activation. Primary microglia were treated with LPS (1 µg/ml) with or without SB203580 (10 µM) or the NLRP3 inflammasome inhibitor glyburide (50 µM) for 8 h and analyzed for LC3 level, caspase-1 activation, and IL-1β production. **(D and E)** Inhibition of ULK1 activity activates microglia. Primary microglia were treated with the ULK1 inhibitor MRT67307 (10 µM) and assayed for various markers and activated caspase-1 (8 h; D) or for morphological changes as described in B (12 h; E). Dashed lines show cell body outlines. Bars, 40 µm. $n = 100$. **(F)** ULK1 mediates LPS-induced caspase-1 activation. ULK1 WT and mutants (504A/757A and ULK1/2A or 504E/757E and ULK1/2E) were transfected into primary microglia. Cells were treated with LPS (1 µg/ml) for 8 h and analyzed for caspase-1 activation. Bars, 20 µm. $n = 50$. **, $P < 0.01$ versus control; ##, $P < 0.01$ versus LPS. $n = 3$. Error bars show SD.

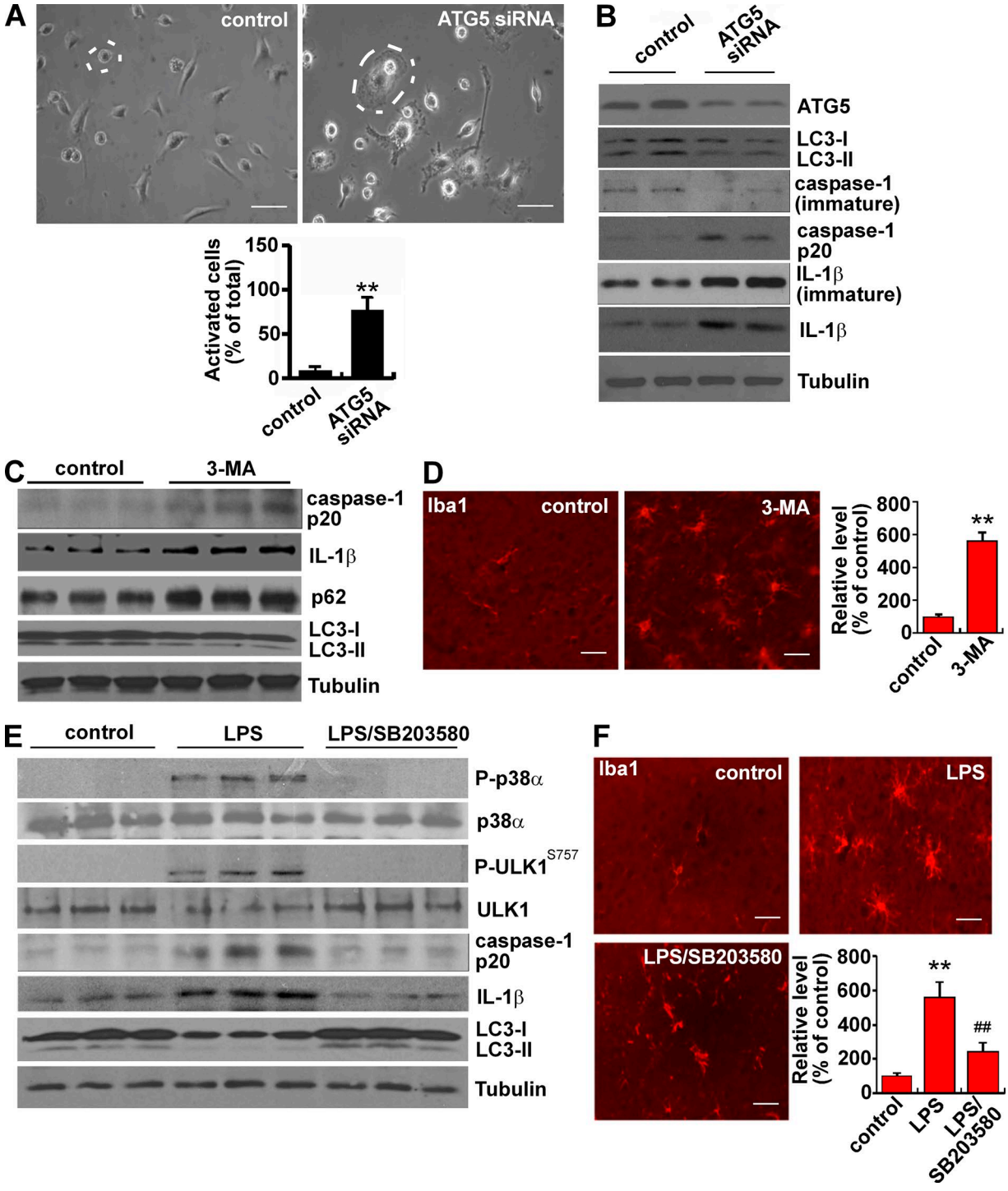

Figure 7. **LPS activates microglia through p38α-mediated inhibition of autophagy. (A)** Knockdown of ATG5 induces morphological change in cultured primary microglia. Primary microglia were transfected with ATG5 siRNA (10 nM) for 48 h and scored for process retraction and cell body enlargement. Dashed lines show cell body outlines. Bars, 40 µm. *n* = 100. The below graph shows the percentage of cells with retracted processes and enlarged cell bodies. **(B)** Knockdown of ATG5 inhibits autophagy and induces caspase-1 activation. Primary microglia were transfected with ATG5 siRNA (10 nM) for 36 h and analyzed for LC3 level, caspase-1 activation, and IL-1β production. **(C and D)** Inhibition of autophagy activates microglia in the mouse brain. 3-MA was injected via i.p. (10 mg/kg/d) into 1-mo-old CD1 mice. After 2 d, cortical brain tissues were dissected for Western blotting (C), or whole animals were perfused with saline and 4% paraformaldehyde for Iba1 immunostaining (D). **(E and F)** SB203580 blocks LPS-induced inhibition of autophagy and microglia activation in mouse brains. LPS (5 µg/side; I.C.V.) was injected into 1-mo-old CD1 mice. SB203580 (2 mg/animal; i.p.) was injected 2 h before and 0 h after LPS admission. 24 h later, cortical brain tissues were dissected for Western blotting (E), or whole animals were perfused with saline and 4% paraformaldehyde for Iba1 immunostaining (F). Bars, 50 µm. *n* = 100. **, P < 0.01 versus control; ##, P < 0.01 versus LPS. *n* = 8/group. Experiments were repeated three times. Error bars show SD.

of the reason for the difference may be the cellular models used. Several lines of evidence support this. The basal level of phosphorylation of ULK1 in RAW264.7 was very high compared with that in BV2 cells. Although LPS caused a robust activation of p38 MAPK, this did not appear to lead to an LPS-induced phosphorylation of ULK1 in RAW264.7 cells. In addition, unlike macrophages (Fujita et al., 2011), LPS did not induce transcriptional activation of p62 in microglia. At present, it is unclear whether these differences are related and underlie the observed distinct autophagic response between microglia and macrophages. Regardless, our data suggest that under our experimental conditions, microglia appear to be uniquely capable of linking p38 MAPK signal to ULK1. Because inhibition of ULK1 by MRT67307 in microglia led to the activation of the inflammatory process, it would be interesting to test whether inhibition of ULK1 may trigger a distinct reaction in macrophages and to delineate the specific mechanisms responsible for their unique response.

Our analyses indicate that p38 MAPK phosphorylates ULK1 at two sites: S504, whose modification has not been reported before, and S757, which is also targeted by mTOR (Kim et al., 2011). Therefore, p38 MAPK and mTOR share the inhibitory site S757 to inhibit ULK1. How phosphorylation of ULK1 negatively regulates its interaction with ATG13 is not clear. It is worth noting that structurally, one of the p38 MAPK phosphorylation sites (S757) is located in the microtubule interacting and transport (MIT) domain of ULK1 (Fujioka et al., 2014). The MIT of ATG1, the yeast ULK1 homologue, has been shown to mediate the interaction with ATG13, which is mainly hydrophobic (Fujioka et al., 2014; Noda and Fujioka, 2015). This mode of interaction appears to be conserved between ULK1 and ATG13 in mammals (Fujioka et al., 2014; Papinski and Kraft, 2016). Thus, it is possible that phosphorylation by p38 MAPK in the MIT domain may hinder the hydrophobic interaction between ULK1 and ATG13, disrupting the complex. Because dephosphorylation of ATG13 has been reported to be required for its interaction with ATG1 (Kamada et al., 2000), phosphorylation of ULK1 and ATG13 has emerged as a critical mechanism that regulates ULK1 kinase activity and autophagy.

Our findings raise the question of how autophagy precisely inhibits inflammatory processes in the absence of proinflammatory signal-induced overt p38 MAPK signaling. Our data show that p38 MAPK–ULK1 regulates the levels of both caspase-1 and IL-1β, supporting the theory that inflammasome itself may be one of the likely targets negatively controlled by autophagy. Because the p38 MAPK–ULK1 pathway also modulates microglial morphology, it is possible that autophagy may target several aspects of the inflammatory machinery. The regulatory mechanism defined in this study is important to microglia, and therefore it is likely to be involved in neuroinflammatory diseases (Pena-Altamira et al., 2016).

Materials and methods

Animals

Long-Evans rats and CD1 mice were purchased from Charles River Laboratories. All animal experiments were performed in accordance with Guide for the Care and Use of Laboratory Animals (National Research Council). 3-MA (Sigma-Aldrich) was dissolved in DMSO to make a 10-mg/ml concentrated stock. The 3-MA stock solution was diluted 1:10 in PBS and administered by i.p. injection (10 mg/kg/d; Walter et al., 2014). Ultrapure LPS (Sigma-Aldrich) was dissolved in sterile saline at a concentration of 1 mg/ml. Mice were anesthetized by i.p. injection of a mixture of 200 mg/kg ketamine and 10 mg/kg xylazine. Then, mice were placed into a rodent stereotaxic frame (David Kopf Instruments). The scalp was shaved, and a burr hole was drilled 1 mm caudal to the bregma and 2.0 mm lateral to the midline. LPS (5 µg) was injected via a Hamilton microsyringe into the ventricle over a 5-min period (Zhou et al., 2006). All procedures were approved by the Institutional Animal Care and Use Committee of Emory University.

Antibodies and reagents

Antibodies against p38 MAPK (9218), phospho–p38 MAPK (Thr180/Tyr182; 9211), ULK1 (8054), phospho-ULK1 (Ser757; 6866), ATG13 (6940), LC3A/B (4108), SQSTM1/p62 (5114), MYC-tag (2276), p70S6 (9202), phospho–p70S6 kinase (Thr389; 9206), mTOR (4517), phospho-mTOR (Ser2448; 5536), and cleaved caspase-1 (4199) were obtained from Cell Signaling Technology. Antibodies against FLAG-tag (F1804) were purchased from Sigma-Aldrich. Antibodies against IL-1β (sc-1252), NOS2 (sc-8310), and HA-tag (sc-805) were purchased from Santa Cruz Biotechnology, Inc. Caspase-1 antibody (AG-20B-0042) was from Adipogen. LPS was purchased from Sigma-Aldrich. TLR4 peptide inhibitor set VIPER (IMG-2011A) and the control peptide CP7 (IMG-2011B) were provided by IMGENEX. Plasmid mTagRFP-mWasabi-LC3 was provided by J. Lin (Peking University). Kinase active p38 protein (14-337) was from EMD Millipore.

DNA constructs

MYC-ULK1 and HA-ULK1 expression plasmids were purchased from Addgene. Mutations were performed using the QuikChange Mutagenesis kit from Agilent Technologies. Primers used for mutations are the following: S504A forward, 5′-GTCCCTACACACCTGCTCCCCAAG TGGGA-3′, and S504A reverse, 5′-TCCCACTTGGGGAGCAGG TGTGTAGGGAC-3′; S757A forward, 5′-GTATTTACTGTAGGC GCCCCACCCAGTGGTG-3′, and S757A reverse 5′-GTGGTATTT ACTGTAGGCTCCCCACCCAGTGGTGCCA-3′; S504E forward, 5′-GTGGCCGTCCCTACACACCTGAGCCCCAAGTGGGAACCAT CCCAG-3′, and S504E reverse 5′-CTGGGATGGTTCCCACTTGGG GCTCAGGTGTGTAGGGACGGCCAC-3′; and S757E forward, 5′-CTGTGGTATTTACTGTAGGCGAGCCACCCAGTGGTGCCACCC CAC-3′, and S757E reverse, 5′-GTGGGGTGGCACCACTGGGTG GCTCGCCTACAGTAAATACCACAG-3′.

Cell culture

Primary microglia were prepared from whole brains of P2 *Long-Evans* rat pups or CD1 mouse pups (Xing et al., 2011). Disassociated brain cells were seeded onto 150-cm^2 flasks and maintained in DMEM/F-12 supplemented with 10% FBS, 2 mM L-glutamine, 1 mM sodium pyruvate, and 0.1 mM nonessential amino acids. The medium was changed every 3 d. Microglia were isolated by shaking the flasks containing confluent mixed-glia cultures for 3 h at 150 rpm. The BV2 microglial cells were cultured in DMEM/F-12 medium (Invitrogen) containing 5% FBS (Invitrogen) and 50 µg/ml penicillin/streptomycin. HEK293T cells were cultured in DMEM (Invitrogen) culture medium containing 10% FBS (Invitrogen) and 50 µg/ml penicillin/streptomycin.

Plasmid transfection

Plasmids were transfected into HEK293T cells using Lipofectamine 2000 reagent (Invitrogen).

In vitro p38α kinase assay

In vitro p38α kinase assay was performed following the manufacturer's instructions. In brief, ULK1 proteins were immunoprecipitated

from cells with either anti-MYC (Cell Signaling Technology) or anti-ULK1 (Santa Cruz Biotechnology, Inc.) antibodies. Then, the immunoprecipitation (IP) products were washed three times with IP buffer (10% glycerol, 50 mM Tris, pH 7.7, 150 mM NaCl, 0.5% NP-40, 1× DTT, 1× protease inhibitors, and 0.1 µM okadaic acid) followed by 1× kinase buffer (25 mM Tris-HCl, pH 7.5, 5 mM β-glycerophosphate, 2 mM DTT, 0.1 mM Na_3VO_4, and 10 mM $MgCl_2$). The immunoprecipitated products were incubated with 100 ng p38α MAPK in kinase buffer containing 25 µM cold ATP with or without 2 µCi [γ-^{32}P]ATP under 30°C for 30 min, and the reaction was terminated by adding SDS sample buffer, heated at 95°C for 5 min, and then subjected to SDS-PAGE and autoradiography.

In vitro ULK1 kinase assay

Endogenous ULK1 or recombinant ULK1 were immunoprecipitated with either anti-MYC (Cell Signaling Technology) or anti-ULK1 (sc-10900; Santa Cruz Biotechnology, Inc.) antibodies as indicated. The immune complexes were extensively washed with lysis buffer followed by washing with kinase buffer. The immunoprecipitated ULK1 beads were incubated with 3 µg MBP in kinase buffer containing 25 µM cold ATP and 2 µCi[γ-^{32}P]ATP per reaction. The kinase reaction was performed in 30°C for 30 min, and the reaction was terminated by adding SDS sample buffer, heated at 95°C for 5 min, and subjected to SDS-PAGE and autoradiography.

Quantitative real-time PCR (qRT-PCR)

Total RNA was isolated using a TRIzol isolation kit. Whole cDNA was synthesized from 1 µg of purified RNA by the SuperScript II First-Strand cDNA synthesis system (Invitrogen). Primer sequences for p62 qRT-PCR were described previously by Hu et al. (2012). The qRT-PCR was performed with SYBR green brilliant III ultrafast reagent kit (MX3000P; Agilent Technologies) following the manufacturer's protocol. The results of qRT-PCR assays presented are a mean of three independent RNA preparations. Each sample was analyzed in triplicates.

Caspase-1 and IL-1β quantification

Secreted caspase-1 and IL-1β in the cell culture media were quantified with ELISA kits from Adipogen and Abcam, respectively, following the manufacturers' procedures. The caspase-1 assay included the following steps: adding 100 µl of the different standards or cell culture supernatant samples into a 96-well plate in duplicate, incubating for 2 h at room temperature, aspirating the coated wells and washing with 300 µl of wash buffer five times, adding 100 µl of the diluted detection antibody, incubating for 1 h at room temperature, washing with 300 µl of wash buffer five times, adding 100 µl to each well of the diluted HRP-labeled streptavidin for 30 min incubation at room temperature, washing with 300 µl of wash buffer five times, adding 100 µl of 3,3',5,5'-tetramethylbenzidine (TMB) substrate solution for 20 min color reaction at room temperature, stopping the reaction by adding 50 µl of stop solution, and measuring the OD at 450 nm in a microplate reader (Bio-Tek). The IL-1β assay included the following steps: adding 100 µl of each standard and sample into a 96-well plate, incubating for 2.5 h at room temperature with gentle shaking, washing four times with 1× wash solution, incubating with 100 µl of 1× biotinylated IL-1β detection antibody for 1 h at room temperature with gentle shaking, repeating the wash step, adding 100 µl of 1× HRP-streptavidin solution for 45 min incubation at room temperature with gentle shaking, washing as above, adding 100 µl of TMB one-step substrate reagent for 30 min incubation at room temperature in the dark with gentle shaking, adding 50 µl of stop solution, and reading at 450 nm in a microplate reader immediately.

co-IP assay

Cells lysates (200–400 µg) were prepared in IP buffer (20 mM Tris-HCl, pH 7.4, 150 mM NaCl, 2 mM $MgCl_2$, 1% [vol/vol] Triton X-100, 0.5% sodium deoxycholate, and cocktail protease inhibitors) and incubated with Protein A/G beads (GE Healthcare) at 4°C for 1 h with gentle rotation. After centrifugation at 500 *g* for 1 min, the precleaned lysates were incubated with the appropriate antibody at 4°C for 12 h with gentle rotation. The Protein-A/G beads were added and incubated for another 3 h. Immunoprecipitates were collected by centrifugation at 500 *g* for 1 min, washed three times with IP buffer, and then heated at 95°C for 5 min in 20 µl sample buffer (31.5 mM Tris-HCl, pH 6.8, 10% glycerol, 1% SDS, and 0.005% bromophenol blue) for SDS-PAGE.

Western blotting

Western blotting was performed as previously described (She et al., 2011). Whole-cell lysates were prepared in SDS containing sample buffer (31.5 mM Tris-HCl, pH 6.8, 10% glycerol, 1% SDS, and 0.005% bromophenol blue), and equal amounts of lysates (20–30 µg) were separated by 10–15% SDS-PAGE gel at 100 V for 1.5 h. Proteins were transferred to polyvinylidene difluoride membrane at 25 V for 1.5 h using a half-dry blotting system (Bio-Rad Laboratories). Blots were probed by incubation with first antibodies (1:1,000) overnight at 4°C, washed three times, and then incubated with the second antibodies (1:10,000) at room temperature for 1 h. Images were developed in an M35A X-OMAT Processor system (Kodak) using ECL reagent (GE Healthcare).

Immunocytochemistry/immunohistochemistry

Cells were fixed with 4% formalin containing 0.1% Triton X-100 in PBS for 10 min at room temperature. After washing three times with PBS, the coverslips were incubated with blocking buffer (PBS containing 5% goat serum, 3% BSA [Thermo Fisher Scientific], and 0.1% Triton X-100) for 30 min at room temperature. Primary antibodies were diluted in blocking buffer and incubated with the cells at room temperature for 2 h. For detection of primary antibodies, species-appropriate Alexa Fluor fluorescently conjugated secondary antibodies (1:1,000; Invitrogen) were incubated in blocking buffer at room temperature for 2 h. Widefield fluorescent photomicrographs were obtained using an Axioplan 2 microscope with an Axiocam MRc5 digital camera (ZEI SS). For immunohistochemistry, fixed brain tissues were sliced into 40-µm sections. After washing three times with PBS, the slices were incubated with blocking buffer for 30 min at room temperature. Primary antibodies were diluted 1:200 in blocking buffer and incubated with the cells at 4°C overnight. Incubation with secondary antibody (1:500) and image taking were done as same as immunocytochemistry.

Statistical analysis

Data are presented as means ± SD. Comparison between two groups was analyzed using two-tailed Student's *t* tests, and two-way ANOVAs with general linear model procedures using a univariate approach were applied for more than two groups. All statistical analyses were performed with SPSS software. A p-value of >0.05 was considered significant.

Online supplemental material

Fig. S1 shows how LPS inhibits autophagy in microglia but not in RAW264.7 cells. Fig. S2 shows how LPS inhibits autophagy in BV2 cells through p38α MAPK. Fig. S3 shows how p38α MAPK phosphorylates ULK1. Fig. S4 shows how p38α MAPK inhibits ULK1 activity. Fig. S5 shows how the LPS-induced inflammatory response in BV2 cells and primary microglia correlates closely with a reduction of LC3-II levels. Fig. S6 shows how inhibition of autophagy induces inflammation in primary microglia and in vivo.

Acknowledgments

This work was supported by the BrightFocus Foundation and National Institutes of Health grants AG023695, NS079858, P50 AG025688 pilot, and NS095269 to Z. Mao, the National Natural Science Foundation of China grant 81570528 to Y. He, and the China Scholarship Council grant 201606095029 to T. Zhang.

The authors declare no competing financial interests.

Author contributions: Z. Mao designed and oversaw the study. Y. He, H. She, M. Yepes, Y. Zhao, and Z. Mao designed the experiments. Y. He, H. She, T. Zhang, H. Xu, and L. Cheng performed and analyzed the experiments. Y. He, H. She, and Z. Mao wrote the manuscript with feedback from other authors.

Submitted: 6 January 2017
Revised: 30 July 2017
Accepted: 30 October 2017

References

Bachstetter, A.D., and L.J. Van Eldik. 2010. The p38 MAP Kinase Family as Regulators of Proinflammatory Cytokine Production in Degenerative Diseases of the CNS. *Aging Dis.* 1:199–211.

Bachstetter, A.D., B. Xing, L. de Almeida, E.R. Dimayuga, D.M. Watterson, and L.J. Van Eldik. 2011. Microglial p38α MAPK is a key regulator of proinflammatory cytokine up-regulation induced by toll-like receptor (TLR) ligands or beta-amyloid (Aβ). *J. Neuroinflammation.* 8:79. https://doi.org/10.1186/1742-2094-8-79

Blasi, E., R. Barluzzi, V. Bocchini, R. Mazzolla, and F. Bistoni. 1990. Immortalization of murine microglial cells by a v-raf/v-myc carrying retrovirus. *J. Neuroimmunol.* 27:229–237. https://doi.org/10.1016/0165-5728(90)90073-V

Chan, E.Y., A. Longatti, N.C. McKnight, and S.A. Tooze. 2009. Kinase-inactivated ULK proteins inhibit autophagy via their conserved C-terminal domains using an Atg13-independent mechanism. *Mol. Cell. Biol.* 29:157–171. https://doi.org/10.1128/MCB.01082-08

Delgado, M.A., R.A. Elmaoued, A.S. Davis, G. Kyei, and V. Deretic. 2008. Toll-like receptors control autophagy. *EMBO J.* 27:1110–1121. https://doi.org/10.1038/emboj.2008.31

Deretic, V., T. Saitoh, and S. Akira. 2013. Autophagy in infection, inflammation and immunity. *Nat. Rev. Immunol.* 13:722–737. https://doi.org/10.1038/nri3532

Doyle, A., G. Zhang, E.A. Abdel Fattah, N.T. Eissa, and Y.P. Li. 2011. Toll-like receptor 4 mediates lipopolysaccharide-induced muscle catabolism via coordinate activation of ubiquitin-proteasome and autophagy-lysosome pathways. *FASEB J.* 25:99–110. https://doi.org/10.1096/fj.10-164152

Fujioka, Y., S.W. Suzuki, H. Yamamoto, C. Kondo-Kakuta, Y. Kimura, H. Hirano, R. Akada, F. Inagaki, Y. Ohsumi, and N.N. Noda. 2014. Structural basis of starvation-induced assembly of the autophagy initiation complex. *Nat. Struct. Mol. Biol.* 21:513–521. https://doi.org/10.1038/nsmb.2822

Fujita, K., D. Maeda, Q. Xiao, and S.M. Srinivasula. 2011. Nrf2-mediated induction of p62 controls Toll-like receptor-4-driven aggresome-like induced structure formation and autophagic degradation. *Proc. Natl. Acad. Sci. USA.* 108:1427–1432. https://doi.org/10.1073/pnas.1014156108

Harris, J., M. Hartman, C. Roche, S.G. Zeng, A. O'Shea, F.A. Sharp, E.M. Lambe, E.M. Creagh, D.T. Golenbock, J. Tschopp, et al. 2011. Autophagy controls IL-1beta secretion by targeting pro-IL-1beta for degradation. *J. Biol. Chem.* 286:9587–9597. https://doi.org/10.1074/jbc.M110.202911

Hosokawa, N., T. Hara, T. Kaizuka, C. Kishi, A. Takamura, Y. Miura, S. Iemura, T. Natsume, K. Takehana, N. Yamada, et al. 2009. Nutrient-dependent mTORC1 association with the ULK1-Atg13-FIP200 complex required for autophagy. *Mol. Biol. Cell.* 20:1981–1991. https://doi.org/10.1091/mbc.E08-12-1248

Hu, Y.L., M. DeLay, A. Jahangiri, A.M. Molinaro, S.D. Rose, W.S. Carbonell, and M.K. Aghi. 2012. Hypoxia-induced autophagy promotes tumor cell survival and adaptation to antiangiogenic treatment in glioblastoma. *Cancer Res.* 72:1773–1783. https://doi.org/10.1158/0008-5472.CAN-11-3831

Iwai-Kanai, E., H. Yuan, C. Huang, M.R. Sayen, C.N. Perry-Garza, L. Kim, and R.A. Gottlieb. 2008. A method to measure cardiac autophagic flux in vivo. *Autophagy.* 4:322–329. https://doi.org/10.4161/auto.5603

Jain, A., T. Lamark, E. Sjøttem, K.B. Larsen, J.A. Awuh, A. Øvervatn, M. McMahon, J.D. Hayes, and T. Johansen. 2010. p62/SQSTM1 is a target gene for transcription factor NRF2 and creates a positive feedback loop by inducing antioxidant response element-driven gene transcription. *J. Biol. Chem.* 285:22576–22591. https://doi.org/10.1074/jbc.M110.118976

Kamada, Y., T. Funakoshi, T. Shintani, K. Nagano, M. Ohsumi, and Y. Ohsumi. 2000. Tor-mediated induction of autophagy via an Apg1 protein kinase complex. *J. Cell Biol.* 150:1507–1513. https://doi.org/10.1083/jcb.150.6.1507

Kettenmann, H., U.K. Hanisch, M. Noda, and A. Verkhratsky. 2011. Physiology of microglia. *Physiol. Rev.* 91:461–553. https://doi.org/10.1152/physrev.00011.2010

Kim, J., M. Kundu, B. Viollet, and K.L. Guan. 2011. AMPK and mTOR regulate autophagy through direct phosphorylation of Ulk1. *Nat. Cell Biol.* 13:132–141. https://doi.org/10.1038/ncb2152

Kimura, S., T. Noda, and T. Yoshimori. 2007. Dissection of the autophagosome maturation process by a novel reporter protein, tandem fluorescent-tagged LC3. *Autophagy.* 3:452–460. https://doi.org/10.4161/auto.4451

Klionsky, D.J., F.C. Abdalla, H. Abeliovich, R.T. Abraham, A. Acevedo-Arozena, K. Adeli, L. Agholme, M. Agnello, P. Agostinis, J.A. Aguirre-Ghiso, et al. 2012. Guidelines for the use and interpretation of assays for monitoring autophagy. *Autophagy.* 8:445–544. https://doi.org/10.4161/auto.19496

Lamkanfi, M., J.L. Mueller, A.C. Vitari, S. Misaghi, A. Fedorova, K. Deshayes, W.P. Lee, H.M. Hoffman, and V.M. Dixit. 2009. Glyburide inhibits the Cryopyrin/Nalp3 inflammasome. *J. Cell Biol.* 187:61–70. https://doi.org/10.1083/jcb.200903124

Lapaquette, P., M.A. Bringer, and A. Darfeuille-Michaud. 2012. Defects in autophagy favour adherent-invasive Escherichia coli persistence within macrophages leading to increased pro-inflammatory response. *Cell. Microbiol.* 14:791–807. https://doi.org/10.1111/j.1462-5822.2012.01768.x

Levine, B., N. Mizushima, and H.W. Virgin. 2011. Autophagy in immunity and inflammation. *Nature.* 469:323–335. https://doi.org/10.1038/nature09782

Matsuzawa, T., B.H. Kim, A.R. Shenoy, S. Kamitani, M. Miyake, and J.D. Macmicking. 2012. IFN-γ elicits macrophage autophagy via the p38 MAPK signaling pathway. *J. Immunol.* 189:813–818. https://doi.org/10.4049/jimmunol.1102041

Mizushima, N., T. Yoshimori, and B. Levine. 2010. Methods in mammalian autophagy research. *Cell.* 140:313–326. https://doi.org/10.1016/j.cell.2010.01.028

Netea-Maier, R.T., T.S. Plantinga, F.L. van de Veerdonk, J.W. Smit, and M.G. Netea. 2016. Modulation of inflammation by autophagy: Consequences for human disease. *Autophagy.* 12:245–260. https://doi.org/10.1080/15548627.2015.1071759

Noda, N.N., and Y. Fujioka. 2015. Atg1 family kinases in autophagy initiation. *Cell. Mol. Life Sci.* 72:3083–3096. https://doi.org/10.1007/s00018-015-1917-z

Papinski, D., and C. Kraft. 2016. Regulation of Autophagy By Signaling Through the Atg1/ULK1 Complex. *J. Mol. Biol.* 428(9, 9 Pt A):1725–1741. https://doi.org/10.1016/j.jmb.2016.03.030

Pena-Altamira, E., F. Prati, F. Massenzio, M. Virgili, A. Contestabile, M.L. Bolognesi, and B. Monti. 2016. Changing paradigm to target microglia in neurodegenerative diseases: from anti-inflammatory strategy to active immunomodulation. *Expert Opin. Ther. Targets.* 20:1–14. https://doi.org/10.1517/14728222.2016.1121237

Petherick, K.J., O.J. Conway, C. Mpamhanga, S.A. Osborne, A. Kamal, B. Saxty, and I.G. Ganley. 2015. Pharmacological inhibition of ULK1 kinase blocks mammalian target of rapamycin (mTOR)-dependent autophagy. *J. Biol. Chem.* 290:28726. https://doi.org/10.1074/jbc.A114.627778

Ravindran, R., J. Loebbermann, H.I. Nakaya, N. Khan, H. Ma, L. Gama, D.K. Machiah, B. Lawson, P. Hakimpour, Y.C. Wang, et al. 2016. The amino acid sensor GCN2 controls gut inflammation by inhibiting inflammasome activation. *Nature.* 531:523–527. https://doi.org/10.1038/nature17186

Rubinsztein, D.C., A.M. Cuervo, B. Ravikumar, S. Sarkar, V. Korolchuk, S. Kaushik, and D.J. Klionsky. 2009. In search of an "autophagomometer". *Autophagy.* 5:585–589. https://doi.org/10.4161/auto.5.5.8823

She, H., Q. Yang, K. Shepherd, Y. Smith, G. Miller, C. Testa, and Z. Mao. 2011. Direct regulation of complex I by mitochondrial MEF2D is disrupted in a mouse model of Parkinson disease and in human patients. *J. Clin. Invest.* 121:930–940. https://doi.org/10.1172/JCI43871

Shi, C.S., K. Shenderov, N.N. Huang, J. Kabat, M. Abu-Asab, K.A. Fitzgerald, A. Sher, and J.H. Kehrl. 2012. Activation of autophagy by inflammatory signals limits IL-1β production by targeting ubiquitinated inflammasomes for destruction. *Nat. Immunol.* 13:255–263. https://doi.org/10.1038/ni.2215

Walter, K.M., M.J. Schönenberger, M. Trötzmüller, M. Horn, H.P. Elsässer, A.B. Moser, M.S. Lucas, T. Schwarz, P.A. Gerber, P.L. Faust, et al. 2014. Hif-2α promotes degradation of mammalian peroxisomes by selective autophagy. *Cell Metab.* 20:882–897. https://doi.org/10.1016/j.cmet.2014.09.017

Xing, B., A.D. Bachstetter, and L.J. Van Eldik. 2011. Microglial p38α MAPK is critical for LPS-induced neuron degeneration, through a mechanism involving TNFα. *Mol. Neurodegener.* 6:84. https://doi.org/10.1186/1750-1326-6-84

Xu, Y., C. Jagannath, X.D. Liu, A. Sharafkhaneh, K.E. Kolodziejska, and N.T. Eissa. 2007. Toll-like receptor 4 is a sensor for autophagy associated with innate immunity. *Immunity.* 27:135–144. https://doi.org/10.1016/j.immuni.2007.05.022

Yamamoto, A., Y. Tagawa, T. Yoshimori, Y. Moriyama, R. Masaki, and Y. Tashiro. 1998. Bafilomycin A1 prevents maturation of autophagic vacuoles by inhibiting fusion between autophagosomes and lysosomes in rat hepatoma cell line, H-4-II-E cells. *Cell Struct. Funct.* 23:33–42. https://doi.org/10.1247/csf.23.33

Zhou, C., W. Zhong, J. Zhou, F. Sheng, Z. Fang, Y. Wei, Y. Chen, X. Deng, B. Xia, and J. Lin. 2012. Monitoring autophagic flux by an improved tandem fluorescent-tagged LC3 (mTagRFP-mWasabi-LC3) reveals that high-dose rapamycin impairs autophagic flux in cancer cells. *Autophagy.* 8:1215–1226. https://doi.org/10.4161/auto.20284

Zhou, H., B.M. Lapointe, S.R. Clark, L. Zbytnuik, and P. Kubes. 2006. A requirement for microglial TLR4 in leukocyte recruitment into brain in response to lipopolysaccharide. *J. Immunol.* 177:8103–8110. https://doi.org/10.4049/jimmunol.177.11.8103

Zhou, R., A.S. Yazdi, P. Menu, and J. Tschopp. 2011. A role for mitochondria in NLRP3 inflammasome activation. *Nature.* 469:221–225. https://doi.org/10.1038/nature09663

Zhu, C.B., A.M. Carneiro, W.R. Dostmann, W.A. Hewlett, and R.D. Blakely. 2005. p38 MAPK activation elevates serotonin transport activity via a trafficking-independent, protein phosphatase 2A-dependent process. *J. Biol. Chem.* 280:15649–15658. https://doi.org/10.1074/jbc.M410858200